Fractional-Order SEIR Model for COVID-19: Finite-Time Stability Analysis and Numerical Validation

Shaher Momani[1,2], Iqbal M. Batiha[2,3,*], Mohammad S. Hijazi[4], Issam Bendib[5], Adel Ouannas[6], Nidal Anakira[7,8]

[1]Department of Mathematics, School of Science, The University of Jordan, Amman, 11942, Jordan
[2]Nonlinear Dynamics Research Center (NDRC), Ajman University, Ajman 346, UAE
[3]Department of Mathematics, Al Zaytoonah University of Jordan, Amman 11733, Jordan
[4]Department of Mathematics, College of Sciences, Jouf University, Sakaka, Saudi Arabia
[5]Applied Mathematics & Modeling Laboratory, Department of Mathematics, Faculty of Exact Sciences, University of Brothers Mentouri, Constantine 25000, Algeria
[6]Department of Mathematics and Computer Science, University of Oum El Bouaghi, Oum El Bouaghi 04000, Algeria
[7]Faculty of Education and Arts, Sohar University, Sohar 3111, Oman
[8]Applied Science Research Center, Applied Science Private University, Amman 11937, Jordan

Emails: s.momani@ju.edu.jo; i.batiha@zuj.edu.jo; Mshijazi@ju.edu.sa; bendib.issam@doc.umc.edu.dz; ouannas.adel@univ-oeb.dz; nanakira@su.edu.om

Abstract

This paper investigates a fractional-order SEIR model to study the dynamics of infectious diseases, specifically COVID-19, by incorporating memory effects through fractional derivatives. The model's formulation enhances the understanding of epidemic dynamics by considering disease transmission, recovery, and mortality rates under fractional calculus. Stability analyses are conducted for the disease-free equilibrium (DFE) and the pandemic fixed point (PFP), identifying critical conditions for finite-time stability using Lyapunov functions and fractional derivatives. Numerical simulations validate theoretical findings, demonstrating finite-time stabilization around the equilibrium points under realistic parameter settings. The results underscore the advantages of fractional-order modeling in capturing complex epidemic dynamics and highlight its potential to inform public health intervention strategies.

Keywords: Fractional-order SEIR model; COVID-19 dynamics; Finite-time stability; Epidemic modeling; Lyapunov functions; Disease-free equilibrium; Pandemic fixed point

1 Introduction

Coronavirus disease 2019 (COVID-19), caused by the SARS-CoV-2 virus, was first identified in Wuhan, China, in December 2019.[1] The virus primarily spreads through respiratory droplets and close contact, with an incubation period of approximately 2–14 days.[2] Common symptoms include fever, cough, fatigue, and shortness of breath, though some cases remain asymptomatic. While most infections are mild, approximately 20 % of cases develop moderate to severe symptoms, with around 5 % progressing to pneumonia, acute respiratory distress syndrome, and multi-organ dysfunction. Elderly individuals and those with pre-existing health conditions are at higher risk for severe outcomes. Diagnosis typically involves molecular testing of respiratory samples, with CT imaging used in some cases.[2] Supportive care remains the primary treatment, as no specific antiviral therapy has been widely adopted. Preventive measures include isolation for mild cases and rigorous infection control in healthcare facilities.

Mathematical modeling has been crucial in forecasting COVID-19 transmission and evaluating public health interventions. Various modeling approaches have been applied, including machine learning techniques and compartmental models such as the Susceptible-Infectious-Recovered (SIR) model, as well as models that incorporate behavioral adaptations. These models estimate transmission rates, predict epidemic peaks, and assess outbreak durations. Compartmental models, which segment populations into epidemiological classes, are frequently used to examine the effects of interventions like lockdowns, quarantines, and hospital capacity on epidemic spread. A key parameter in these models is the basic reproduction number (R_0), where $R_0 < 1$ indicates the potential for disease extinction through local asymptotic stability of the disease-free equilibrium.[3] Sensitivity analyses of model parameters provide insights into optimal intervention strategies, with consensus suggesting that sustained non-pharmaceutical interventions are essential for pandemic control. These models, therefore, offer vital guidance to policymakers for developing effective measures to mitigate COVID-19 spread.

Advances in epidemic modeling have integrated network theory to address the complexities of disease propagation within interconnected populations. Researchers have employed heterogeneous mean-field and pair-quenched mean-field approaches to study epidemic dynamics across single-layer and multilayer networks.[4] This interdisciplinary approach combines network theory and epidemiology, enabling the development of statistical tools for parameter estimation from observed networks and simulation methods for tracking disease dynamics. These models offer valuable insights into disease spread patterns and have contributed to improved epidemic control and prevention.

Compartmental models have become foundational for understanding infectious disease dynamics, particularly during the COVID-19 pandemic. These models classify populations by disease status, facilitating the examination of disease transmission and the effectiveness of control measures. Modified versions of compartmental models incorporate public health interventions such as lockdowns, mask usage, and vaccination.[5] Additionally,[6] provides an extensive overview of compartmental models tailored to COVID-19, including variants integrating non-pharmaceutical interventions. Beyond compartmental frameworks, agent-based and network models have also advanced our understanding of COVID-19 spread. Recently, fractional-order SEIR models, which account for memory effects,[7,8] have shown promise in capturing complex epidemic dynamics with improved accuracy compared to traditional models. Applied to various infectious diseases, including COVID-19 and Ebola, these models enhance predictive precision and reduce errors, with stability analyses highlighting parameters critical to epidemic outcomes.

Research on COVID-19 dynamics has also explored discrete and fractional-order adaptations of traditional models. SIR and SEIR models, for example, have been used to assess transmission rates and forecast the pandemic's trajectory. Some studies have compared more complex models derived from SEIR to simpler ones like SIRD to evaluate prediction reliability. Spatially explicit models have also been developed to investigate disease pathways and simulate the effects of policy interventions.[9] Comparative studies have analyzed models such as the Hawkes point process and SEIR frameworks to assess their effectiveness in capturing COVID-19 spread.[10]

Fractional-order models are increasingly recognized for their ability to represent COVID-19 dynamics more accurately. For instance, in a stochastic SIR framework,[11] applied finite-time stability analysis to determine disease persistence or eradication criteria while evaluating control interventions.[12] proposed an efficient computational approach for fractional-order COVID-19 models, emphasizing both computational efficiency and long-term behavioral insights. These studies underscore the value of fractional-order models in capturing intricate COVID-19 dynamics, providing essential tools for understanding and forecasting the pandemic's progression.

This paper is organized as follows: Section 2 introduces the foundational concepts of fractional-order systems, including definitions, theoretical preliminaries, and the mathematical framework required for stability analysis. Section 3 describes the SEIR model, including its classical and fractional-order formulations, and outlines the key parameters and equilibrium points. Section 4 focuses on the finite-time stability analysis of the fractional-order SEIR model, presenting theoretical results and critical conditions for stability at the Disease-Free Equilibrium (DFE) and the Pandemic Fixed Point (PFP). Section 5 validates the theoretical findings through numerical simulations, demonstrating the model's dynamics under different parameter configurations and illustrating finite-time stabilization.

2 Foundational Concepts

Consider a category of fractional-order nonlinear systems (FONS) represented using the Caputo fractional-order derivative (CFOD) as follows:

$$ {}_{t_0}^{C}D_{\mathfrak{t}}^{\gamma}\mathfrak{f}(\mathfrak{t}) = \bar{\chi}(\mathfrak{t}, \mathfrak{f}(\mathfrak{t})) \tag{1} $$

with the initial condition $\mathfrak{f}(\mathfrak{t}_0) = \mathfrak{f}_0$, where $\mathfrak{f} \in \mathbb{R}^n$, $\gamma \in (0,1)$, and $\bar{\chi}(\mathfrak{t}, \mathfrak{f}(\mathfrak{t})) : [\mathfrak{t}_0, +\infty) \times \Omega \to \mathbb{R}^n$. Here, $\Omega \subset \mathbb{R}^n$ is an interval containing $\mathfrak{f} = 0$, and $\bar{\chi}(\mathfrak{t}, \mathfrak{f}(\mathfrak{t}))$ is piecewise continuous in $\mathfrak{t}$ over the interval $[\mathfrak{t}_0, +\infty)$.

This study aims to define the equation for the finite-time equilibrium point (FTEP), denoted by $\mathfrak{f}_\mathfrak{e}$, of the FONS and to establish sufficient conditions that ensure the FTS of this equilibrium point $\mathfrak{f}_\mathfrak{e}$.

Definition 1. *For a function $\mathfrak{f}(\mathfrak{t})$, $\mathfrak{t} \in [\mathfrak{t}_0, +\infty)$, the fractional-order integral $I_{\mathfrak{t}_0}^{-\gamma}\mathfrak{f}(\mathfrak{t})(\gamma > 0)$ is defined as*

$$ {}_{\mathfrak{t}_0}I_{\mathfrak{t}}^{\gamma}\mathfrak{f}(\mathfrak{t}) = \frac{1}{\Gamma(\gamma)} \int_{\mathfrak{t}_0}^{\mathfrak{t}} (\mathfrak{t} - \vartheta)^{\gamma - 1} \mathfrak{f}(\vartheta)\, d\vartheta. \tag{2} $$

Definition 2. *For a function $\mathfrak{f}(\mathfrak{t})$, $\mathfrak{t} \in [\mathfrak{t}_0, +\infty)$, the Riemann–Liouville fractional-order derivative ${}_{\mathfrak{t}_0}^{R}D_{\mathfrak{t}}^{\gamma}\mathfrak{f}(\mathfrak{t})$, is defined as*

$$ {}_{\mathfrak{t}_0}^{R}D_{\mathfrak{t}}^{\gamma}\mathfrak{f}(\mathfrak{t}) = \frac{d}{d\mathfrak{t}} I_{\mathfrak{t}}^{1-\gamma}\mathfrak{f}(\mathfrak{t}) = \frac{1}{\Gamma(1-\gamma)} \frac{d}{d\mathfrak{t}} \int_{\mathfrak{t}_0}^{\mathfrak{t}} \frac{\mathfrak{f}(\vartheta)}{(\mathfrak{t} - \vartheta)^{\gamma}}\, d\vartheta, \tag{3} $$

where $\gamma \in (0,1)$.

Definition 3. *For a function $\mathfrak{f}(\mathfrak{t}) \in C^1[\mathfrak{t}_0, +\infty)$, the CFOD ${}_{\mathfrak{t}_0}^{C}D_{\mathfrak{t}}^{\gamma}\mathfrak{f}(\mathfrak{t}), \gamma \in (0,1)$ is defined as*

$$ {}_{\mathfrak{t}_0}^{C}D_{\mathfrak{t}}^{\gamma}\mathfrak{f}(\mathfrak{t}) = I_{\mathfrak{t}}^{1-\gamma}\dot{\mathfrak{f}}(\mathfrak{t}) = \frac{1}{\Gamma(1-\gamma)} \int_{\mathfrak{t}_0}^{\mathfrak{t}} \frac{\dot{\mathfrak{f}}(\vartheta)}{(\mathfrak{t} - \vartheta)^{\gamma}}\, d\vartheta. \tag{4} $$

where $\dot{\mathfrak{f}}$ is the first-order derivative of the function $\mathfrak{f}(\mathfrak{t})$.

Lemma 1 ([13])**.** *For ${}_{\mathfrak{t}_0}^{C}D_{\mathfrak{t}}^{\gamma}\mathfrak{f}(\mathfrak{t})$ with $\gamma \in (0,1)$, we have*

$$ {}_{\mathfrak{t}_0}I_{\mathfrak{t}}^{\gamma}\, {}_{\mathfrak{t}_0}^{C}D_{\mathfrak{t}}^{\gamma}\mathfrak{f}(\mathfrak{t}) = \mathfrak{f}(\mathfrak{t}) - \mathfrak{f}(\mathfrak{t}_0). \tag{5} $$

Definition 4 ([13])**.** *$\mathfrak{f}_\mathfrak{e}$ is called a FTEP of the FONS if there exists a $\mathfrak{t}_\mathfrak{e} > \mathfrak{t}_0$ such that $\mathfrak{f}(\mathfrak{t}) \neq \mathfrak{f}_\mathfrak{e}$ for $\mathfrak{t} \in [\mathfrak{t}_0, \mathfrak{t}_\mathfrak{e})$, and $\mathfrak{f}(\mathfrak{t}) \equiv \mathfrak{f}_\mathfrak{e}$ for $\mathfrak{t} \in [\mathfrak{t}_\mathfrak{e}, +\infty)$.*

Theorem 2.1 ([13])**.** *If $\mathfrak{f}_\mathfrak{e}$ is an FTEP of the FONS, ${}_{\mathfrak{t}_0}^{C}D_{\mathfrak{t}}^{\gamma}\mathfrak{f}(\mathfrak{t}) = \chi(\mathfrak{t}, \mathfrak{f}(\mathfrak{t}))$ is continuous on $[\mathfrak{t}_0, +\infty)$, then*

$$ {}_{\mathfrak{t}_0}^{C}D_{\mathfrak{t}}^{\gamma}\mathfrak{f}(\mathfrak{t}) = \bar{\chi}(\mathfrak{t}, \mathfrak{f}_\mathfrak{e}) \not\equiv 0, \quad \forall \mathfrak{t} \in [\mathfrak{t}_\mathfrak{e}, +\infty). \tag{6} $$

Definition 5 ([13])**.** *If there exists a constant $\mathfrak{t}_\mathfrak{e} > \mathfrak{t}_0$, such that*

$$ {}_{\mathfrak{t}_\mathfrak{e}}^{C}D_{\mathfrak{t}}^{\gamma}\mathfrak{f}(\mathfrak{t}) = {}_{\mathfrak{t}_\mathfrak{e}}^{C}D_{\mathfrak{t}}^{\gamma}\mathfrak{f}_\mathfrak{e} = \bar{\chi}(\mathfrak{t}, \mathfrak{f}_\mathfrak{e}) \equiv 0, \quad \mathfrak{t} \in [\mathfrak{t}_\mathfrak{e}, +\infty). \tag{7} $$

then $\mathfrak{f}_\mathfrak{e} = \mathfrak{f}(\mathfrak{t}_\mathfrak{e})$ is called the FTEP of the FONS.

Theorem 2.2 ([13])**.** *$\mathfrak{f}_\mathfrak{e} = \mathfrak{f}(\mathfrak{t}_\mathfrak{e})$ is an FTEP of the FONS if and only if there exists a $\mathfrak{t}_\mathfrak{e} > \mathfrak{t}_0$, such that*

$$ {}_{\mathfrak{t}_0}^{C}D_{\mathfrak{t}}^{\gamma}\mathfrak{f}(\mathfrak{t}) = \frac{1}{\Gamma(1-\gamma)} \int_{\mathfrak{t}_0}^{\mathfrak{t}_\mathfrak{e}} (\mathfrak{t} - \vartheta)^{-\gamma} \dot{\mathfrak{f}}(\vartheta)\, d\vartheta, \quad \forall \mathfrak{t} > \mathfrak{t}_\mathfrak{e}. \tag{8} $$

Lemma 2. *Assume that $\mathfrak{f}(\mathfrak{t})$ is a continuous differentiable function. Then, the following inequality holds for any time instant $t \geq \mathfrak{t}_0$:*

$$ \frac{1}{2}\, {}_{\mathfrak{t}_0}^{C}D_{t}^{\gamma}\mathfrak{f}^2(t) \leq \mathfrak{f}(\mathfrak{t})\, {}_{0}^{C}D_{\mathfrak{t}}^{\gamma}\mathfrak{f}(\mathfrak{t}), \quad 0 < \gamma < 1. \tag{9} $$

Lemma 3. *There exists a positive constant C such that*

$$ |\bar{\mathfrak{f}}\bar{\mathfrak{g}} - \mathfrak{f}\mathfrak{g}| \leq \mathsf{C}(|\bar{\mathfrak{f}} - \mathfrak{f}| + |\bar{\mathfrak{g}} - \mathfrak{g}|). \tag{10} $$

Proof. To initiate this proof, we start by providing an estimate for the term $|\bar{\mathfrak{f}}\bar{\mathfrak{g}} - \mathfrak{f}\mathfrak{g}|$ as shown below:

$$\begin{aligned} |\bar{\mathfrak{f}}\bar{\mathfrak{g}} - \mathfrak{f}\mathfrak{g}| &= |\bar{\mathfrak{f}}\bar{\mathfrak{g}} - \mathfrak{f}\bar{\mathfrak{g}} + \mathfrak{f}\bar{\mathfrak{g}} - \mathfrak{f}\mathfrak{g}| \\ &\leq |\bar{\mathfrak{g}}||\bar{\mathfrak{f}} - \mathfrak{f}| + |\mathfrak{f}||\bar{\mathfrak{g}} - \mathfrak{g}| \\ &\leq \ell_1|\bar{\mathfrak{f}} - \mathfrak{f}| + \ell_2|\bar{\mathfrak{g}} - \mathfrak{g}| \\ &\leq \mathsf{C}(|\bar{\mathfrak{f}} - \mathfrak{f}| + |\bar{\mathfrak{g}} - \mathfrak{g}|). \end{aligned} \tag{11}$$

where $\mathsf{C} = \max\{\ell_1, \ell_2\}$. □

Theorem 2.3 ([14]). *Let $\mathfrak{f} = 0$ be an equilibrium point of the VFO system* (1)*, and let $\mathcal{D} \subset \mathbb{R}^n$ denote a domain containing the origin. Assume there exists a continuously differentiable function $\mathtt{V}(\mathfrak{t}, \mathfrak{f}(\mathfrak{t})) : [\mathfrak{t}_0, \infty) \times \mathcal{D} \to \mathbb{R}$ such that, for any positive constants Λ_1, Λ_2, Λ_3, $\mathfrak{a}$, and $\mathfrak{b}$, the following conditions are met:*

$$\begin{cases} \Lambda_1\|\mathfrak{f}\|^{\mathfrak{a}} \leq \mathtt{V}(\mathfrak{t}, \mathfrak{f}(\mathfrak{t})) \leq \Lambda_2\|\mathfrak{f}\|^{\mathfrak{a}\mathfrak{b}}, \\ {}_{\mathfrak{t}_0}^{C}D^{\gamma}\mathtt{V}(\mathfrak{t}, \mathfrak{f}(\mathfrak{t})) \leq -\Lambda_3\|\mathfrak{f}\|^{\mathfrak{a}\mathfrak{b}}, \end{cases} \tag{12}$$

where $\mathfrak{f} \in \mathcal{D}$, $0 < \gamma < 1$, and $\mathfrak{t} \in [\mathfrak{t}_0, \infty)$.

Theorem 2.4 ([14]). *Let $\mathtt{V}(\mathfrak{t})$ be a continuous function that is positive definite. Suppose that it satisfies the condition:*

$${}_{\mathfrak{t}_0}^{C}D_{\mathfrak{t}}^{\gamma}\mathtt{V}(\mathfrak{t}) \leq -\Lambda\mathtt{V}(\mathfrak{t}) \quad \textit{for } \mathfrak{t} \geq \mathfrak{t}_0, \tag{13}$$

where Λ is a positive constant. Under these assumptions, the following inequality holds:

$$\mathtt{V}(\mathfrak{t}) \leq \mathtt{V}(\mathfrak{t}_0)\mathsf{e}_{\gamma}\left(-\Lambda\mathfrak{t}^{\gamma}\right) \tag{14}$$

for $\mathfrak{t}_0 \leq \mathfrak{t} < \mathfrak{t}_{\mathfrak{e}}$, where $\mathfrak{t}_{\mathfrak{e}} = \left(\dfrac{\gamma+1}{\Lambda}\right)^{\dfrac{1}{\gamma-1}}$. The function $\mathsf{e}_{\gamma}(\mathfrak{t})$ is the Mittag-Leffler function, defined as:

$$\mathsf{e}_{\gamma}(\mathfrak{t}) = \sum_{k=0}^{\infty} \frac{\mathfrak{t}^k}{\Gamma(\gamma k + 1)}. \tag{15}$$

Additionally, it is required that $\mathtt{V}(\mathfrak{t}_0) \geq 0$ for any specified $\mathfrak{t}_0$, and that $\mathtt{V}(\mathfrak{t}) = 0$ for $\mathfrak{t} \geq \mathfrak{t}_{\mathfrak{e}}$.

Definition 6. *Suppose $\mathcal{D} \subseteq \Omega$ is an open interval containing 0. If there is a function $\mathfrak{t}_{\mathfrak{e}} : \mathcal{D} \setminus \{0\} \to (0, +\infty)$ called the settling time function satisfying the following conditions:*

1. *For all $\mathfrak{f}_0 \in \mathcal{D} \setminus \{0\}$, $\mathfrak{f}(\mathfrak{t}) = \mathfrak{f}(\mathfrak{t}, \mathfrak{t}_0, \mathfrak{f}_0) \in \mathcal{D} \setminus \{0\}$ for all $\mathfrak{t} \in [0, \mathfrak{t}_{\mathfrak{e}}(\mathfrak{f}_0))$, and $\lim\limits_{\mathfrak{t} \to \mathfrak{t}_{\mathfrak{e}}(\mathfrak{f}_0)} \mathfrak{f}(\mathfrak{t}) = 0$.*
2. *For every open neighborhood U_{ε} of 0, there is an open subset U_{δ} containing 0 in $\mathcal{D}$, satisfying that for all $\mathfrak{f}_0 \in U_{\delta} \setminus \{0\}$ and $\mathfrak{t} \in [0, \mathfrak{t}_{\mathfrak{e}}(\mathfrak{f}_0))$, $\mathfrak{f}(\mathfrak{t}) \in U_{\varepsilon} \setminus \{0\}$.*

The equilibrium point 0 of the FONS is then said to be finite-time stable.

3 Model Description

The SEIR model is widely utilized in epidemiology, including COVID-19 studies, to classify individuals into Susceptible, Exposed, Infectious, and Recovered compartments. This model incorporates transmission and recovery rates and mortality rates to simulate epidemic dynamics.[15,16] While SEIR models can effectively predict equilibrium states, they can sometimes underestimate peak infection rates and overestimate epidemic duration due to simplifying assumptions about time spent within compartments.[17] Consequently, researchers have introduced modifications, such as incorporating vaccination, temporary immunity, or discrete-time stochastic frameworks, to enhance accuracy.[18] Applied across various countries to project COVID-19 progression and assess non-pharmaceutical interventions, this model has revealed spatiotemporal variations in transmission

and recovery rates. Despite its limitations, the SEIR model remains essential for epidemic forecasting and analysis.

Recent advancements in epidemic modeling, motivated by the COVID-19 pandemic, include using fractional-order derivatives in SEIR and SIR models, particularly those of commensurate order. These fractional models better capture the nonlinear and memory-dependent nature, accounting for memory effects and anomalous diffusion observed in real-world data.[19] Analytical studies have explored the existence, uniqueness, and stability using tools such as the Picard-Lindelöf theorem and Lyapunov functions. Stability analyses at disease-free and endemic equilibrium points have identified critical parameters influencing epidemic outcomes, offering insights into threshold conditions and the potential persistence of diseases. Numerical simulations support these theoretical findings, highlighting the influence of fractional orders on disease dynamics and informing more effective intervention strategies. To increase realism, some models now incorporate compartments for preventive measures, which have proven effective in reducing COVID-19 transmission risk. These adaptations underscore the need for flexible epidemic models to address evolving public health challenges.

The classical SEIR model is formulated as follows:

$$\begin{cases} \dfrac{d\mathtt{S}}{d\mathtt{t}} = \lambda - \mathfrak{r}_1 \dfrac{\mathtt{S}(\mathtt{t})\mathtt{E}(\mathtt{t})}{N(\mathtt{t})} - \mathfrak{r}_2 \dfrac{\mathtt{S}(\mathtt{t})\mathtt{I}(\mathtt{t})}{N(\mathtt{t})} - \eta \mathtt{S}(\mathtt{t}) + \vartheta \mathtt{R}(\mathtt{t}), \\ \dfrac{d\mathtt{E}}{d\mathtt{t}} = \mathfrak{r}_1 \dfrac{\mathtt{S}(\mathtt{t})\mathtt{E}(\mathtt{t})}{N(\mathtt{t})} + \mathfrak{r}_2 \dfrac{\mathtt{S}(\mathtt{t})\mathtt{I}(\mathtt{t})}{N(\mathtt{t})} - (\eta + \nu)\mathtt{E}(\mathtt{t}), \\ \dfrac{d\mathtt{I}}{d\mathtt{t}} = \nu \mathtt{E}(\mathtt{t}) - (\zeta + \mathfrak{d} + \eta)\mathtt{I}(\mathtt{t}), \\ \dfrac{d\mathtt{R}}{d\mathtt{t}} = \zeta \mathtt{I}(\mathtt{t}) - (\eta + \vartheta)\mathtt{R}(\mathtt{t}). \end{cases} \tag{16}$$

In this model, the compartments $\mathtt{S}(\mathtt{t})$, $\mathtt{E}(\mathtt{t})$, $\mathtt{I}(\mathtt{t})$, and $\mathtt{R}(t)$ represent the susceptible, exposed, infectious, and recovered populations, respectively.

Key parameters for understanding the model's dynamics include:

- λ: recruitment rate into the susceptible population,
- $\mathfrak{r}_1$ and $\mathfrak{r}_2$: incidence rates for contracting infection,
- η: natural mortality rate unrelated to the epidemic,
- ϑ: relapse rate, indicating the probability of recovered individuals becoming infectious again,
- ν: progression rate from exposed to infectious,
- ζ: recovery rate for infectious individuals,
- $\mathfrak{d}$: disease-specific mortality rate for COVID-19.

This framework is a comprehensive foundation for analyzing disease transmission and recovery dynamics.

Fractional calculus has garnered attention for its applicability in modeling complex phenomena across various fields, including epidemiology. Studies on fractional-order models for diseases like anthroponotic cutaneous leishmaniasis,[20] tuberculosis,[21] and visceral leishmaniasis[22] have demonstrated enhanced accuracy when compared to integer-order models, often employing the Caputo fractional derivative. Researchers have applied mathematical techniques, like fixed-point theory and stability analysis, to explore these models. Fractional-order approaches provide a deeper understanding of disease dynamics' complexity. The field's growth has spurred the development of new numerical methods and toolkits, facilitating the application of fractional calculus in diverse domains.[23]

The fractional-order SEIR model is given by:

$$\begin{cases} {}_0^C D_{\mathtt{t}}^{\gamma}\mathtt{S}(\mathtt{t}) = \lambda - \mathfrak{r}_1 \dfrac{\mathtt{S}(\mathtt{t})\mathtt{E}(\mathtt{t})}{\mathtt{N}(\mathtt{t})} - \mathfrak{r}_2 \dfrac{\mathtt{S}(\mathtt{t})\mathtt{I}(\mathtt{t})}{\mathtt{N}(\mathtt{t})} - \eta\mathtt{S}(\mathtt{t}) + \vartheta\mathtt{R}(\mathtt{t}), \\ {}_0^C D_{\mathtt{t}}^{\gamma}\mathtt{E}(\mathtt{t}) = \mathfrak{r}_1 \dfrac{\mathtt{S}(\mathtt{t})\mathtt{E}(\mathtt{t})}{\mathtt{N}(\mathtt{t})} + \mathfrak{r}_2 \dfrac{\mathtt{S}(\mathtt{t})\mathtt{I}(\mathtt{t})}{\mathtt{N}(\mathtt{t})} - (\eta+\nu)\mathtt{E}(\mathtt{t}), \\ {}_0^C D_{\mathtt{t}}^{\gamma}\mathtt{I}(\mathtt{t}) = \nu\mathtt{E}(\mathtt{t}) - (\zeta + \mathfrak{d} + \eta)\mathtt{I}(\mathtt{t}), \\ {}_0^C D_{\mathtt{t}}^{\gamma}\mathtt{R}(\mathtt{t}) = \zeta\mathtt{I}(\mathtt{t}) - (\eta+\vartheta)\mathtt{R}(\mathtt{t}), \end{cases} \tag{17}$$

with initial conditions:

$$\begin{aligned} \mathtt{S}(0), \mathtt{E}(0), \mathtt{I}(0), \mathtt{R}(0) \geq 0, \\ \mathtt{N}(\mathtt{t}) = \mathtt{S}(\mathtt{t}) + \mathtt{E}(\mathtt{t}) + \mathtt{I}(\mathtt{t}) + \mathtt{R}(\mathtt{t}), \end{aligned} \tag{18}$$

where $0 < \gamma < 1$.

We can express system (17) in the classical form as follows:

$$\begin{cases} {}_0^C D_{\mathtt{t}}^{\gamma}\mathtt{S}(\mathtt{t}) = \chi_1(\mathtt{t}, \mathtt{S}(\mathtt{t}), \mathtt{E}(\mathtt{t}), \mathtt{I}(\mathtt{t}), \mathtt{R}(\mathtt{t})), \\ {}_0^C D_{\mathtt{t}}^{\gamma}\mathtt{E}(\mathtt{t}) = \chi_2(\mathtt{t}, \mathtt{S}(\mathtt{t}), \mathtt{E}(\mathtt{t}), \mathtt{I}(\mathtt{t}), \mathtt{R}(\mathtt{t})), \\ {}_0^C D_{\mathtt{t}}^{\gamma}\mathtt{I}(\mathtt{t}) = \chi_3(\mathtt{t}, \mathtt{S}(\mathtt{t}), \mathtt{E}(\mathtt{t}), \mathtt{I}(\mathtt{t}), \mathtt{R}(\mathtt{t})), \\ {}_0^C D_{\mathtt{t}}^{\gamma}\mathtt{R}(\mathtt{t}) = \chi_4(\mathtt{t}, \mathtt{S}(\mathtt{t}), \mathtt{E}(\mathtt{t}), \mathtt{I}(\mathtt{t}), \mathtt{R}(\mathtt{t})). \end{cases} \tag{19}$$

Here, the functions χ_i for $i = 1, 2, 3, 4$ are defined as follows:

$$\begin{cases} \chi_1(\mathtt{t}, \mathtt{S}(\mathtt{t}), \mathtt{E}(\mathtt{t}), \mathtt{I}(\mathtt{t}), \mathtt{R}(\mathtt{t})) = \lambda - \mathfrak{r}_1 \dfrac{\mathtt{S}(\mathtt{t})\mathtt{E}(\mathtt{t})}{\mathtt{N}(\mathtt{t})} - \mathfrak{r}_2 \dfrac{\mathtt{S}(\mathtt{t})\mathtt{I}(\mathtt{t})}{\mathtt{N}(\mathtt{t})} - \eta\mathtt{S}(\mathtt{t}) + \vartheta\mathtt{R}(\mathtt{t}), \\ \chi_2(\mathtt{t}, \mathtt{S}(\mathtt{t}), \mathtt{E}(\mathtt{t}), \mathtt{I}(\mathtt{t}), \mathtt{R}(\mathtt{t})) = \mathfrak{r}_1 \dfrac{\mathtt{S}(\mathtt{t})\mathtt{E}(\mathtt{t})}{\mathtt{N}(\mathtt{t})} + \mathfrak{r}_2 \dfrac{\mathtt{S}(\mathtt{t})\mathtt{I}(\mathtt{t})}{\mathtt{N}(\mathtt{t})} - (\eta+\nu)\mathtt{E}(\mathtt{t}), \\ \chi_3(\mathtt{t}, \mathtt{S}(\mathtt{t}), \mathtt{E}(\mathtt{t}), \mathtt{I}(\mathtt{t}), \mathtt{R}(\mathtt{t})) = \nu\mathtt{E}(\mathtt{t}) - (\zeta + \mathfrak{d} + \eta)\mathtt{I}(\mathtt{t}), \\ \chi_4(\mathtt{t}, \mathtt{S}(\mathtt{t}), \mathtt{E}(\mathtt{t}), \mathtt{I}(\mathtt{t}), \mathtt{R}(\mathtt{t})) = \zeta\mathtt{I}(\mathtt{t}) - (\eta+\vartheta)\mathtt{R}(\mathtt{t}). \end{cases} \tag{20}$$

4 Finite-Time Stability Analysis of the Model

Recent advances in the study of FTEP of equilibrium points in fractional-order nonlinear systems (FONSs) have revealed some contrasting findings. For example,[24] demonstrated the non-existence of finite-time stable equilibria in FONSs without time delays. In contrast,[25] contested this result, providing evidence for the existence of finite-time stable equilibrium points. This work introduced a unified definition for FTS in FONSs and sufficient conditions for achieving stability. Other researchers have examined fractional-order systems that include time delays. For instance,[26] derived new criteria for FTS in nonlinear fractional-order systems with time delays, utilizing techniques such as the Laplace transform and the Mittag-Leffler function. Similarly,[27]

explored FTS conditions in fractional-order BAM neural networks with time delays, applying methods like the Bellman-Gronwall inequality and contraction mapping. These studies contribute significantly to the ongoing discourse on FTS in fractional-order systems.

This section establishes several FTS analysis results for the fractional-order COVID-19 model, specifically as described in equation (17). Our study identifies two critical equilibrium points: Disease-Free Equilibrium (DFE) and the Pandemic Fixed Point.

The following equations define the system:

$$\begin{cases} \lambda - \mathfrak{r}_1 \dfrac{\mathtt{S}^*\mathtt{E}^*}{\mathtt{N}^*} - \mathfrak{r}_2 \dfrac{\mathtt{S}^*\mathtt{I}^*}{\mathtt{N}^*} - \eta \mathtt{S}^* + \vartheta \mathtt{R}^* = 0, \\ \mathfrak{r}_1 \dfrac{\mathtt{S}^*\mathtt{E}^*}{\mathtt{N}^*} + \mathfrak{r}_2 \dfrac{\mathtt{S}^*\mathtt{I}^*}{\mathtt{N}^*} - (\eta + \nu)\mathtt{E}^* = 0, \\ \nu \mathtt{E}^* - (\zeta + \mathfrak{d} + \eta)\mathtt{I}^* = 0, \\ \zeta \mathtt{I}^* - (\eta + \vartheta)\mathtt{R}^* = 0. \end{cases} \tag{21}$$

From these equations, we identify the equilibrium points:

- The Disease-Free Equilibrium (DFE), denoted as $\mathcal{E}_0 = \left(\dfrac{\lambda}{\eta}, 0, 0, 0\right)$, which represents a scenario where the infection has been eradicated.
- The Pandemic Fixed Point, $\mathcal{E}_1 = (\mathtt{S}_1^*, \mathtt{E}_1^*, \mathtt{I}_1^*, \mathtt{R}_1^*)$, characterized by the following expressions:

$$\mathtt{I}_1^* = \frac{\nu}{\zeta + \mathfrak{d} + \eta}\, \mathtt{E}^*,$$

$$\mathtt{R}_1^* = \frac{\zeta\nu}{(\eta + \vartheta)(\zeta + \mathfrak{d} + \eta)}\, \mathtt{E}^*,$$

$$\mathtt{S}_1^* = \frac{1}{\eta}\left(\lambda + \left(\frac{\zeta\vartheta\nu}{(\eta + \vartheta)(\zeta + \mathfrak{d} + \eta)} - (\eta + \nu)\right)\mathtt{E}^*\right).$$

These equilibrium points will be used to further analyze the finite-time stability of the fractional-order COVID-19 model under various parameter configurations, contributing to a deeper understanding of the disease dynamics.

Theorem 4.1. Let $(\mathtt{S}^*, \mathtt{E}^*, \mathtt{I}^*, \mathtt{R}^*)$ be a FTEP of system (17), which is continuous on $[0, +\infty)$. Then, for all $\mathfrak{t} \geq \mathfrak{t}_\epsilon$, we have:

$$\begin{cases} {}_0^C D_{\mathfrak{t}}^{\gamma} \mathtt{S}(\mathfrak{t}) = \chi_1(\mathfrak{t}, \mathtt{S}^*, \mathtt{E}^*, \mathtt{I}^*, \mathtt{R}^*) \not\equiv 0, \\ {}_0^C D_{\mathfrak{t}}^{\gamma} \mathtt{E}(\mathfrak{t}) = \chi_2(\mathfrak{t}, \mathtt{S}^*, \mathtt{E}^*, \mathtt{I}^*, \mathtt{R}^*) \not\equiv 0, \\ {}_0^C D_{\mathfrak{t}}^{\gamma} \mathtt{I}(\mathfrak{t}) = \chi_3(\mathfrak{t}, \mathtt{S}^*, \mathtt{E}^*, \mathtt{I}^*, \mathtt{R}^*) \not\equiv 0, \\ {}_0^C D_{\mathfrak{t}}^{\gamma} \mathtt{R}(\mathfrak{t}) = \chi_4(\mathfrak{t}, \mathtt{S}^*, \mathtt{E}^*, \mathtt{I}^*, \mathtt{R}^*) \not\equiv 0. \end{cases} \tag{22}$$

Proof. We demonstrate this proof by contradiction. Assume that for $\mathfrak{t} \in [\mathfrak{t}_\epsilon, +\infty)$, we have:

$$\begin{cases} {}_0^C D_{\mathfrak{t}}^{\gamma} \mathtt{S}(\mathfrak{t}) = \chi_1(\mathfrak{t}, \mathtt{S}^*, \mathtt{E}^*, \mathtt{I}^*, \mathtt{R}^*) = 0, \\ {}_0^C D_{\mathfrak{t}}^{\gamma} \mathtt{E}(\mathfrak{t}) = \chi_2(\mathfrak{t}, \mathtt{S}^*, \mathtt{E}^*, \mathtt{I}^*, \mathtt{R}^*) = 0, \\ {}_0^C D_{\mathfrak{t}}^{\gamma} \mathtt{I}(\mathfrak{t}) = \chi_3(\mathfrak{t}, \mathtt{S}^*, \mathtt{E}^*, \mathtt{I}^*, \mathtt{R}^*) = 0, \\ {}_0^C D_{\mathfrak{t}}^{\gamma} \mathtt{R}(\mathfrak{t}) = \chi_4(\mathfrak{t}, \mathtt{S}^*, \mathtt{E}^*, \mathtt{I}^*, \mathtt{R}^*) = 0. \end{cases} \tag{23}$$

According to Lemma 1, for all $\mathfrak{t} \geq \mathfrak{t}_\mathfrak{e}$, we have $(\mathtt{S}(\mathfrak{t}), \mathtt{E}(\mathfrak{t}), \mathtt{I}(\mathfrak{t}), \mathtt{R}(\mathfrak{t})) = (\mathtt{S}^*, \mathtt{E}^*, \mathtt{I}^*, \mathtt{R}^*)$, and thus

$$\begin{aligned}
&|\mathtt{S}^* - \mathtt{S}(0)| + |\mathtt{E}^* - \mathtt{E}(0)| + |\mathtt{I}^* - \mathtt{I}(0)| + |\mathtt{R}^* - \mathtt{R}(0)| \\
&= \left|{}_0I_\mathfrak{t}^\gamma {}_0^C D_\mathfrak{t}^\gamma \mathtt{S}(\mathfrak{t})\right| + \left|{}_0I_\mathfrak{t}^\gamma {}_0^C D_\mathfrak{t}^\gamma \mathtt{E}(\mathfrak{t})\right| + \left|{}_0I_\mathfrak{t}^\gamma {}_0^C D_\mathfrak{t}^\gamma \mathtt{I}(\mathfrak{t})\right| + \left|{}_0I_\mathfrak{t}^\gamma {}_0^C D_\mathfrak{t}^\gamma \mathtt{R}(\mathfrak{t})\right| \\
&= \frac{1}{\Gamma(\gamma)} \sum_{i=1}^{4} \left| \int_0^\mathfrak{t} (\mathfrak{t} - \vartheta)^{\gamma-1} \chi_i(\mathfrak{t}, \mathtt{S}^*, \mathtt{E}^*, \mathtt{I}^*, \mathtt{R}^*)\, d\vartheta \right| \\
&= \frac{1}{\Gamma(\gamma)} \sum_{i=1}^{4} \left(\left| \int_0^{\mathfrak{t}_\mathfrak{e}} (\mathfrak{t} - \vartheta)^{\gamma-1} \chi_i(\mathfrak{t}, \mathtt{S}^*, \mathtt{E}^*, \mathtt{I}^*, \mathtt{R}^*)\, d\vartheta + \int_{\mathfrak{t}_\mathfrak{e}}^\mathfrak{t} (\mathfrak{t} - \vartheta)^{\gamma-1} \chi_i(\mathfrak{t}, \mathtt{S}^*, \mathtt{E}^*, \mathtt{I}^*, \mathtt{R}^*)\, d\vartheta \right| \right) \\
&\leq \frac{1}{\Gamma(\gamma)} \int_0^{\mathfrak{t}_\mathfrak{e}} (\mathfrak{t} - \vartheta)^{\gamma-1} \sum_{i=1}^{4} |\chi_i(\mathfrak{t}, \mathtt{S}^*, \mathtt{E}^*, \mathtt{I}^*, \mathtt{R}^*)|\, d\vartheta.
\end{aligned} \tag{24}$$

Given that $\chi_i(\mathfrak{t}, \mathtt{S}^*, \mathtt{E}^*, \mathtt{I}^*, \mathtt{R}^*)$ is continuous over the closed interval $[0, \mathfrak{t}_\mathfrak{e}]$, it follows that it is bounded on this interval. Therefore, there exists a constant $\mathfrak{c} > 0$ such that

$$|\chi_i(\mathfrak{t}, \mathtt{S}^*, \mathtt{E}^*, \mathtt{I}^*, \mathtt{R}^*)| \leq \mathfrak{c} \quad \text{for all} \quad \mathfrak{t} \in [0, \mathfrak{t}_\mathfrak{e}].$$

Thus,

$$|\mathtt{S}^* - \mathtt{S}(0)| + |\mathtt{E}^* - \mathtt{E}(0)| + |\mathtt{I}^* - \mathtt{I}(0)| + |\mathtt{R}^* - \mathtt{R}(0)| \leq \frac{4\mathfrak{c}}{\Gamma(\gamma+1)} \left[\mathfrak{t}^\gamma - (\mathfrak{t} - \mathfrak{t}_\mathfrak{e})^\gamma\right]. \tag{25}$$

By the Mean-Value Theorem,[28] we find:

$$\mathfrak{t}^\gamma - (\mathfrak{t} - \mathfrak{t}_\mathfrak{e})^\gamma \leq \gamma \mathfrak{t}_\mathfrak{e} \aleph^{\gamma-1}, \quad \mathfrak{t} - \mathfrak{t}_\mathfrak{e} < \aleph < \mathfrak{t}. \tag{26}$$

As $\mathfrak{t} \to +\infty$ (i.e., $\aleph \to +\infty$), we obtain:

$$\begin{aligned}
\lim_{\mathfrak{t} \to +\infty} |\mathtt{S}^* - \mathtt{S}(0)| + |\mathtt{E}^* - \mathtt{E}(0)| + |\mathtt{I}^* - \mathtt{I}(0)| + |\mathtt{R}^* - \mathtt{R}(0)| &\leq \lim_{\mathfrak{t} \to +\infty} \frac{4\mathfrak{c}\mathfrak{t}_\mathfrak{e}}{\Gamma(\gamma)} \aleph^{\gamma-1} \\
&= \lim_{\aleph \to +\infty} \frac{4\mathfrak{c}\mathfrak{t}_\mathfrak{e}}{\Gamma(\gamma)} \aleph^{\gamma-1} = 0.
\end{aligned} \tag{27}$$

This implies that for all $\mathfrak{t} \geq \mathfrak{t}_\mathfrak{e}$, we have:

$$(\mathtt{S}(0), \mathtt{E}(0), \mathtt{I}(0), \mathtt{R}(0)) = (\mathtt{S}^*, \mathtt{E}^*, \mathtt{I}^*, \mathtt{R}^*). \tag{28}$$

This contradicts Definition 4 and Theorem 2.1. Therefore, we conclude:

$$\begin{cases}
{}_0^C D_\mathfrak{t}^\gamma \mathtt{S}(\mathfrak{t}) = \chi_1(\mathfrak{t}, \mathtt{S}^*, \mathtt{E}^*, \mathtt{I}^*, \mathtt{R}^*) \not\equiv 0, \\
{}_0^C D_\mathfrak{t}^\gamma \mathtt{E}(\mathfrak{t}) = \chi_2(\mathfrak{t}, \mathtt{S}^*, \mathtt{E}^*, \mathtt{I}^*, \mathtt{R}^*) \not\equiv 0, \\
{}_0^C D_\mathfrak{t}^\gamma \mathtt{I}(\mathfrak{t}) = \chi_3(\mathfrak{t}, \mathtt{S}^*, \mathtt{E}^*, \mathtt{I}^*, \mathtt{R}^*) \not\equiv 0, \\
{}_0^C D_\mathfrak{t}^\gamma \mathtt{R}(\mathfrak{t}) = \chi_4(\mathfrak{t}, \mathtt{S}^*, \mathtt{E}^*, \mathtt{I}^*, \mathtt{R}^*) \not\equiv 0.
\end{cases} \tag{29}$$

□

Theorem 4.2. $(\mathtt{S}^*, \mathtt{E}^*, \mathtt{I}^*, \mathtt{R}^*) = (\mathtt{S}(\mathfrak{t}), \mathtt{E}(\mathfrak{t}_\mathfrak{e}), \mathtt{I}(\mathfrak{t}_\mathfrak{e}), \mathtt{R}(\mathfrak{t}_\mathfrak{e}))$ is a FTEP of the system (17) if and only if there exists a $\mathfrak{t}_\mathfrak{e} > 0$ such that

$${}_0^C D_\mathfrak{t}^\gamma \mathtt{S}(\mathfrak{t}) + {}_0^C D_\mathfrak{t}^\gamma \mathtt{E}(\mathfrak{t}) + {}_0^C D_\mathfrak{t}^\gamma \mathtt{I}(\mathfrak{t}) + {}_0^C D_\mathfrak{t}^\gamma \mathtt{R}(\mathfrak{t}) = \frac{1}{\Gamma(1-\gamma)} \int_0^{\mathfrak{t}_\mathfrak{e}} \frac{\sum_{i=1}^4 \dot{\chi}_i(\vartheta, \mathtt{S}(\vartheta), \mathtt{E}(\vartheta), \mathtt{I}(\vartheta), \mathtt{R}(\vartheta))}{(\mathfrak{t} - \vartheta)^\gamma}\, d\vartheta, \tag{30}$$

$\forall \mathfrak{t} > \mathfrak{t}_\mathfrak{e}$.

Proof. By Definition 3, we have:

$$\begin{aligned}
{}_0^C D_{\mathtt{t}}^{\gamma}\mathtt{S}(\mathtt{t}) + {}_0^C D_{\mathtt{t}}^{\gamma}\mathtt{E}(\mathtt{t}) + {}_0^C D_{\mathtt{t}}^{\gamma}\mathtt{I}(\mathtt{t}) + {}_0^C D_{\mathtt{t}}^{\gamma}\mathtt{R}(\mathtt{t}) &= \frac{1}{\Gamma(1-\gamma)}\int_0^{\mathtt{t}_\epsilon} \frac{\sum_{i=1}^4 \dot{\chi}_i(\vartheta,\mathtt{S}(\vartheta),\mathtt{E}(\vartheta),\mathtt{I}(\vartheta),\mathtt{R}(\vartheta))}{(\mathtt{t}-\vartheta)^{\gamma}}\,d\vartheta \\
&\quad + \frac{1}{\Gamma(1-\gamma)}\int_{\mathtt{t}_\epsilon}^{\mathtt{t}} \frac{\sum_{i=1}^4 \dot{\chi}_i(\vartheta,\mathtt{S}(\vartheta),\mathtt{E}(\vartheta),\mathtt{I}(\vartheta),\mathtt{R}(\vartheta))}{(\mathtt{t}-\vartheta)^{\gamma}}\,d\vartheta \\
&= \frac{1}{\Gamma(1-\gamma)}\int_0^{\mathtt{t}_\epsilon} \frac{\sum_{i=1}^4 \dot{\chi}_i(\vartheta,\mathtt{S}(\vartheta),\mathtt{E}(\vartheta),\mathtt{I}(\vartheta),\mathtt{R}(\vartheta))}{(\mathtt{t}-\vartheta)^{\gamma}}\,d\vartheta \\
&\quad + \frac{1}{\Gamma(1-\gamma)}\int_{\mathtt{t}_\epsilon}^{\mathtt{t}} \frac{\sum_{i=1}^4 \dot{\chi}_i(\vartheta,\mathtt{S}^*,\mathtt{E}^*,\mathtt{I}^*,\mathtt{R}^*)}{(\mathtt{t}-\vartheta)^{\gamma}}\,d\vartheta \\
&= \frac{1}{\Gamma(1-\gamma)}\int_0^{\mathtt{t}_\epsilon} \frac{\sum_{i=1}^4 \dot{\chi}_i(\vartheta,\mathtt{S}(\vartheta),\mathtt{E}(\vartheta),\mathtt{I}(\vartheta),\mathtt{R}(\vartheta))}{(\mathtt{t}-\vartheta)^{\gamma}}\,d\vartheta.
\end{aligned} \tag{31}$$

which leads to

$${}_{\mathtt{t}_\epsilon}^C D_{\mathtt{t}}^{\gamma}\mathtt{S}(\mathtt{t}) + {}_{\mathtt{t}_\epsilon}^C D_{\mathtt{t}}^{\gamma}\mathtt{E}(\mathtt{t}) + {}_{\mathtt{t}_\epsilon}^C D_{\mathtt{t}}^{\gamma}\mathtt{I}(\mathtt{t}) + {}_{\mathtt{t}_\epsilon}^C D_{\mathtt{t}}^{\gamma}\mathtt{R}(\mathtt{t}) = \sum_{i=1}^4 \chi_i(\vartheta,\mathtt{S}(\mathtt{t}),\mathtt{E}(\mathtt{t}),\mathtt{I}(\mathtt{t}),\mathtt{R}(\mathtt{t})), \quad \forall \mathtt{t} \geq \mathtt{t}_\epsilon. \tag{32}$$

Based on Definition 5. Thus, we derive the following:

$${}_{\mathtt{t}_\epsilon}^C D_{\mathtt{t}}^{\gamma}\mathtt{S}(\mathtt{t}) + {}_{\mathtt{t}_\epsilon}^C D_{\mathtt{t}}^{\gamma}\mathtt{E}(\mathtt{t}) + {}_{\mathtt{t}_\epsilon}^C D_{\mathtt{t}}^{\gamma}\mathtt{I}(\mathtt{t}) + {}_0^C D_{\mathtt{t}}^{\gamma}\mathtt{R}(\mathtt{t}) = \sum_{i=1}^4 \chi_i(\vartheta,\mathtt{S}(\mathtt{t}),\mathtt{E}(\mathtt{t}),\mathtt{I}(\mathtt{t}),\mathtt{R}(\mathtt{t})) \equiv 0, \quad \forall \mathtt{t} \geq \mathtt{t}_\epsilon. \tag{33}$$

Applying Lemma 1, we obtain:

$$\begin{aligned}
&|\mathtt{S}(\mathtt{t}) - \mathtt{S}(\mathtt{t}_\epsilon)| + |\mathtt{E}(\mathtt{t}) - \mathtt{E}(\mathtt{t}_\epsilon)| + |\mathtt{I}(\mathtt{t}) - \mathtt{I}(\mathtt{t}_\epsilon)| + |\mathtt{R}(\mathtt{t}) - \mathtt{R}(\mathtt{t}_\epsilon)| \\
&\quad = \left|{}_{\mathtt{t}_\epsilon} I_{\mathtt{t}}^{\gamma}\, {}_{\mathtt{t}_\epsilon}^C D_{\mathtt{t}}^{\gamma}\mathtt{S}(\mathtt{t})\right| + \left|{}_{\mathtt{t}_\epsilon} I_{\mathtt{t}}^{\gamma}\, {}_{\mathtt{t}_\epsilon}^C D_{\mathtt{t}}^{\gamma}\mathtt{E}(\mathtt{t})\right| + \left|{}_{\mathtt{t}_\epsilon} I_{\mathtt{t}}^{\gamma}\, {}_{\mathtt{t}_\epsilon}^C D_{\mathtt{t}}^{\gamma}\mathtt{I}(\mathtt{t})\right| + \left|{}_{\mathtt{t}_\epsilon} I_{\mathtt{t}}^{\gamma}\, {}_0^C D_{\mathtt{t}}^{\gamma}\mathtt{R}(\mathtt{t})\right| \\
&\quad \leq \frac{1}{\Gamma(\gamma)}\int_{\mathtt{t}_\epsilon}^{\mathtt{t}} \frac{\left|\sum_{i=1}^4 \chi_i(\vartheta,\mathtt{S}(\vartheta),\mathtt{E}(\vartheta),\mathtt{I}(\vartheta),\mathtt{R}(\vartheta))\right|}{(\mathtt{t}-\vartheta)^{1-\gamma}}\,d\vartheta = 0.
\end{aligned} \tag{34}$$

Finally, we conclude that:

$$\begin{cases}
\mathtt{S}(\mathtt{t}) = \mathtt{S}(\mathtt{t}_\epsilon) = \mathtt{S}^*, \\
\mathtt{E}(\mathtt{t}) = \mathtt{E}(\mathtt{t}_\epsilon) = \mathtt{E}^*, \\
\mathtt{I}(\mathtt{t}) = \mathtt{I}(\mathtt{t}_\epsilon) = \mathtt{I}^*, \\
\mathtt{R}(\mathtt{t}) = \mathtt{R}(\mathtt{t}_\epsilon) = \mathtt{R}^*.
\end{cases} \tag{35}$$

Thus, $(\mathtt{S}^*, \mathtt{E}^*, \mathtt{I}^*, \mathtt{R}^*)$ is a FTEP of system (17) as established by Theorem 2.2. □

Theorem 4.3. *The equilibrium point* $(\mathtt{S}^*, \mathtt{E}^*, \mathtt{I}^*, \mathtt{R}^*)$ *of system* (17) *is finite-time stable if the following conditions hold:*

$$\mathtt{N}(\mathtt{t}) \geq \mathtt{N}^*, \tag{36}$$

$$\begin{aligned}
\Lambda^* = \min\Bigg\{ &\eta - \frac{\vartheta}{2} - \frac{(\mathsf{C}_1 + \mathsf{C}_2)\max\{\mathfrak{r}_1, \mathfrak{r}_2\}}{4\mathtt{N}^*}, \eta + \frac{\nu}{2} - \frac{(2\mathsf{C}_1 + \mathsf{C}_2)\max\{\mathfrak{r}_1, \mathfrak{r}_2\}}{8\mathtt{N}^*}, \\
&\mathfrak{d} + \eta + \frac{\zeta - \nu}{2} - \frac{\mathsf{C}_2 \max\{\mathfrak{r}_1, \mathfrak{r}_2\}}{8\mathtt{N}^*}, \eta + \frac{\vartheta - \zeta}{2}\Bigg\} > 0.
\end{aligned} \tag{37}$$

where $\mathsf{C}_1 = \max\{\ell_1^*, \mathtt{S}^*\}$ *and* $\mathsf{C}_2 = \max\{\ell_2^*, \mathtt{S}^*\}$*, given that*

$$\mathtt{E}(\mathtt{t}) < \ell_1^*, \quad \mathtt{I}(\mathtt{t}) < \ell_2^*. \tag{38}$$

Furthermore, the estimated settling time is given by

$$\mathtt{t}_\epsilon = \left(\frac{\gamma + 1}{\Lambda^*}\right)^{\frac{1}{\gamma - 1}}. \tag{39}$$

Proof. Examine the Lyapunov function of the following form:

$$\mathtt{V}(\mathtt{t}) = \frac{1}{2}\left(|\mathtt{S}(\mathtt{t}) - \mathtt{S}^*|^2 + |\mathtt{E}(\mathtt{t}) - \mathtt{E}^*|^2 + |\mathtt{I}(\mathtt{t}) - \mathtt{S}^*|^2 + |\mathtt{R}(\mathtt{t}) - \mathtt{R}^*|^2\right), \tag{40}$$

Applying Lemma 2, the following sequential inequalities are obtained by differentiating $\mathtt{V}$ with respect to time $\mathtt{t}$:

$$\begin{aligned}
{}^{C}_{0}D^{\gamma}_{\mathtt{t}}\mathtt{V}(\mathtt{t}) &\leq (\mathtt{S}(\mathtt{t}) - \mathtt{S}^*)\,{}^{C}_{0}D^{\gamma}_{\mathtt{t}}(\mathtt{S}(\mathtt{t}) - \mathtt{S}^*) + (\mathtt{E}(\mathtt{t}) - \mathtt{E}^*)\,{}^{C}_{0}D^{\gamma}_{\mathtt{t}}(\mathtt{E}(\mathtt{t}) - \mathtt{E}^*) + (\mathtt{I}(\mathtt{t}) - \mathtt{I}^*)\,{}^{C}_{0}D^{\gamma}_{\mathtt{t}}(\mathtt{I}(\mathtt{t}) - \mathtt{I}^*) \\
&\quad + (\mathtt{R}(\mathtt{t}) - \mathtt{R}^*)\,{}^{C}_{0}D^{\gamma}_{\mathtt{t}}(\mathtt{R}(\mathtt{t}) - \mathtt{R}^*) \\
&= (\mathtt{S}(\mathtt{t}) - \mathtt{S}^*)\left[-\mathfrak{r}_1\left(\frac{\mathtt{S}(\mathtt{t})\mathtt{E}(\mathtt{t})}{\mathtt{N}(\mathtt{t})} - \frac{\mathtt{S}^*\mathtt{E}^*}{\mathtt{N}^*}\right) - \mathfrak{r}_2\left(\frac{\mathtt{S}(\mathtt{t})\mathtt{I}(\mathtt{t})}{\mathtt{N}(\mathtt{t})} - \frac{\mathtt{S}^*\mathtt{I}^*}{\mathtt{N}^*}\right) - \eta(\mathtt{S}(\mathtt{t}) - \mathtt{S}^*) + \vartheta(\mathtt{R}(\mathtt{t}) - \mathtt{R}^*)\right] \\
&\quad + (\mathtt{E}(\mathtt{t}) - \mathtt{E}^*)\left[\mathfrak{r}_1\left(\frac{\mathtt{S}(\mathtt{t})\mathtt{E}(\mathtt{t})}{\mathtt{N}(\mathtt{t})} - \frac{\mathtt{S}^*\mathtt{E}^*}{\mathtt{N}^*}\right) + \mathfrak{r}_2\left(\frac{\mathtt{S}(\mathtt{t})\mathtt{I}(\mathtt{t})}{\mathtt{N}(\mathtt{t})} - \frac{\mathtt{S}^*\mathtt{I}^*}{\mathtt{N}^*}\right) - (\eta + \nu)(\mathtt{E}(\mathtt{t}) - \mathtt{E}^*)\right] \\
&\quad + (\mathtt{I}(\mathtt{t}) - \mathtt{I}^*)\left[\nu(\mathtt{E}(\mathtt{t}) - \mathtt{E}^*) - (\zeta + \mathfrak{d} + \eta)(\mathtt{I}(\mathtt{t}) - \mathtt{I}^*)\right] \\
&\quad + (\mathtt{R}(\mathtt{t}) - \mathtt{R}^*)\left[\zeta(\mathtt{I}(\mathtt{t}) - \mathtt{I}^*) - (\eta + \vartheta)(\mathtt{R}(\mathtt{t}) - \mathtt{R}^*)\right] \\
&\leq \max\{\mathfrak{r}_1, \mathfrak{r}_2\}\left(|\mathtt{S}(\mathtt{t}) - \mathtt{S}^*| + |\mathtt{E}(\mathtt{t}) - \mathtt{E}^*|\right)\left(\left|\frac{\mathtt{S}(\mathtt{t})\mathtt{E}(\mathtt{t})}{\mathtt{N}(\mathtt{t})} - \frac{\mathtt{S}^*\mathtt{E}^*}{\mathtt{N}^*}\right| + \left|\frac{\mathtt{S}(\mathtt{t})\mathtt{I}(\mathtt{t})}{\mathtt{N}(\mathtt{t})} - \frac{\mathtt{S}^*\mathtt{I}^*}{\mathtt{N}^*}\right|\right) \\
&\quad - \left(\eta - \frac{\vartheta}{2}\right)(\mathtt{S}(\mathtt{t}) - \mathtt{S}^*)^2 - \left(\eta + \frac{\nu}{2}\right)(\mathtt{E}(\mathtt{t}) - \mathtt{E}^*)^2 - \left(\mathfrak{d} + \eta + \frac{\zeta - \nu}{2}\right)(\mathtt{I}(\mathtt{t}) - \mathtt{I}^*)^2 \\
&\quad - \left(\eta + \frac{\vartheta - \zeta}{2}\right)(\mathtt{R}(\mathtt{t}) - \mathtt{R}^*)^2.
\end{aligned} \tag{41}$$

Assume $\mathtt{N}(\mathtt{t}) \geq \mathtt{N}^*$ and apply Lemma 3. Then,

$$\begin{aligned}
{}^{C}_{0}D^{\gamma}_{\mathtt{t}}\mathtt{V}(\mathtt{t}) &\leq \frac{\max\{\mathfrak{r}_1, \mathfrak{r}_2\}}{\mathtt{N}^*}\left(|\mathtt{S}(\mathtt{t}) - \mathtt{S}^*| + |\mathtt{E}(\mathtt{t}) - \mathtt{E}^*|\right)\left(|\mathtt{S}(\mathtt{t})\mathtt{E}(\mathtt{t}) - \mathtt{S}^*\mathtt{E}^*| + |\mathtt{S}(\mathtt{t})\mathtt{I}(\mathtt{t}) - \mathtt{S}^*\mathtt{I}^*|\right) \\
&\quad - \left(\eta - \frac{\vartheta}{2}\right)(\mathtt{S}(\mathtt{t}) - \mathtt{S}^*)^2 - \left(\eta + \frac{\nu}{2}\right)(\mathtt{E}(\mathtt{t}) - \mathtt{E}^*)^2 - \left(\mathfrak{d} + \eta + \frac{\zeta - \nu}{2}\right)(\mathtt{I}(\mathtt{t}) - \mathtt{I}^*)^2 \\
&\quad - \left(\eta + \frac{\vartheta - \zeta}{2}\right)(\mathtt{R}(\mathtt{t}) - \mathtt{R}^*)^2 \\
&\leq \frac{(2\mathtt{C}_1 + \mathtt{C}_2)\max\{\mathfrak{r}_1, \mathfrak{r}_2\}}{8\mathtt{N}^*}\left(|\mathtt{S}(\mathtt{t}) - \mathtt{S}^*|^2 + |\mathtt{E}(\mathtt{t}) - \mathtt{E}^*|^2\right) \\
&\quad + \frac{\mathtt{C}_2\max\{\mathfrak{r}_1, \mathfrak{r}_2\}}{8\mathtt{N}^*}\left(|\mathtt{S}(\mathtt{t}) - \mathtt{S}^*|^2 + |\mathtt{I}(\mathtt{t}) - \mathtt{I}^*|^2\right) \\
&\quad - \left(\eta - \frac{\vartheta}{2}\right)(\mathtt{S}(\mathtt{t}) - \mathtt{S}^*)^2 - \left(\eta + \frac{\nu}{2}\right)(\mathtt{E}(\mathtt{t}) - \mathtt{E}^*)^2 \\
&\quad - \left(\mathfrak{d} + \eta + \frac{\zeta - \nu}{2}\right)(\mathtt{I}(\mathtt{t}) - \mathtt{I}^*)^2 \\
&\quad - \left(\eta + \frac{\vartheta - \zeta}{2}\right)(\mathtt{R}(\mathtt{t}) - \mathtt{R}^*)^2.
\end{aligned}$$

This implies

$$\begin{aligned}
{}^{C}_{0}D^{\gamma}_{\mathtt{t}}\mathtt{V}(\mathtt{t}) &\leq -\left(\eta - \frac{\vartheta}{2} - \frac{(\mathtt{C}_1 + \mathtt{C}_2)\max\{\mathfrak{r}_1, \mathfrak{r}_2\}}{4\mathtt{N}^*}\right)(\mathtt{S}(\mathtt{t}) - \mathtt{S}^*)^2 \\
&\quad - \left(\eta + \frac{\nu}{2} - \frac{(2\mathtt{C}_1 + \mathtt{C}_2)\max\{\mathfrak{r}_1, \mathfrak{r}_2\}}{8\mathtt{N}^*}\right)(\mathtt{E}(\mathtt{t}) - \mathtt{E}^*)^2 \\
&\quad - \left(\mathfrak{d} + \eta + \frac{\zeta - \nu}{2} - \frac{\mathtt{C}_2\max\{\mathfrak{r}_1, \mathfrak{r}_2\}}{8\mathtt{N}^*}\right)(\mathtt{I}(\mathtt{t}) - \mathtt{I}^*)^2 \\
&\quad - \left(\eta + \frac{\vartheta - \zeta}{2}\right)(\mathtt{R}(\mathtt{t}) - \mathtt{R}^*)^2.
\end{aligned} \tag{42}$$

Based on conditions (43)-(46), we derive:

$$\eta > \frac{\vartheta}{2} + \frac{(\mathtt{C}_1 + \mathtt{C}_2)\max\{\mathfrak{r}_1, \mathfrak{r}_2\}}{4\mathtt{N}^*}, \tag{43}$$

$$\eta + \frac{\nu}{2} > \frac{(2\mathtt{C}_1 + \mathtt{C}_2)\max\{\mathfrak{r}_1, \mathfrak{r}_2\}}{8\mathtt{N}^*}, \tag{44}$$

$$\mathfrak{d} + \eta + \frac{\zeta - \nu}{2} > \frac{\mathtt{C}_2 \max\{\mathfrak{r}_1, \mathfrak{r}_2\}}{8\mathtt{N}^*}, \tag{45}$$

$$\eta + \frac{\vartheta - \zeta}{2} > 0. \tag{46}$$

After that,

$$\begin{aligned} {}^{C}_{0}D^{\gamma}_{\mathfrak{t}}\mathtt{V}(\mathfrak{t}) \leq -2\min\Bigg\{ & \eta - \frac{\vartheta}{2} - \frac{(\mathtt{C}_1 + \mathtt{C}_2)\max\{\mathfrak{r}_1, \mathfrak{r}_2\}}{4\mathtt{N}^*}, \eta + \frac{\nu}{2} - \frac{(2\mathtt{C}_1 + \mathtt{C}_2)\max\{\mathfrak{r}_1, \mathfrak{r}_2\}}{8\mathtt{N}^*}, \\ & \mathfrak{d} + \eta + \frac{\zeta - \nu}{2} - \frac{\mathtt{C}_2 \max\{\mathfrak{r}_1, \mathfrak{r}_2\}}{8\mathtt{N}^*}, \eta + \frac{\vartheta - \zeta}{2} \Bigg\} \mathtt{V}(\mathfrak{t}) = \Lambda^* \mathtt{V}(\mathfrak{t}). \end{aligned} \tag{47}$$

The system (17) achieves global asymptotic stability by Theorem 2.3. Consequently, by applying Theorem 2.4, we obtain:

$$\mathtt{V}(\mathfrak{t}) \leq M(\mathfrak{t}) = \mathtt{V}(0)\mathtt{e}_{\gamma}\left(-\Lambda^* \mathfrak{t}^{\gamma}\right), \quad \text{for} \quad 0 \leq \mathfrak{t} < \mathfrak{t}_{\mathfrak{e}}, \tag{48}$$

where the settling time is defined as follows:

$$\mathfrak{t}_{\mathfrak{e}} = \left(\frac{\gamma + 1}{\Lambda^*}\right)^{\frac{1}{\gamma - 1}}.$$

Moreover,

$$\mathtt{V}(\mathfrak{t}) = 0, \quad \text{for} \quad \mathfrak{t} \geq \mathfrak{t}_{\mathfrak{e}}. \tag{49}$$

According to Definition 6, the equilibrium point $(\mathtt{S}^*, \mathtt{E}^*, \mathtt{I}^*, \mathtt{R}^*)$ of the system FONS (17) is finite-time stable. □

5 Numerical Validation and Stability Analysis of the Fractional-Order SEIR Model

This section focuses on validating the theoretical findings of the fractional-order SEIR model described in System (17). This model incorporates memory effects through fractional derivatives, making it particularly suited to capturing the dynamics of epidemics such as COVID-19.

We present two distinct scenarios for analysis:

- **Disease-Free Equilibrium (DFE):** A scenario representing the eradication of infection within the population.
- **Pandemic Fixed Point (PFP):** A controlled scenario where infections persist at equilibrium but are stabilized.

The selected parameter values, listed in Table 1, align with realistic epidemic dynamics commonly observed in the literature. Numerical simulations are performed using fractional differential equation solvers to demonstrate the finite-time stability of both equilibrium points. For further look about other numerical method, the reader may refer to the references.[29,30] Graphical results are presented to illustrate the temporal evolution of the susceptible ($\mathtt{S}(\mathfrak{t})$), exposed ($\mathtt{E}(\mathfrak{t})$), infectious ($\mathtt{I}(\mathfrak{t})$), and recovered ($\mathtt{R}(\mathfrak{t})$) populations. These simulations corroborate the theoretical stability analyses and provide further insights into the system's dynamics.

Table 1: Parameter Descriptions and Values

Parameter	Description	Value at DFE	Value at PFP
λ	Recruitment rate into susceptible population	0.1	3
r_1	Incidence rate (susceptible-to-exposed)	0.11	0.1
r_2	Incidence rate (susceptible-to-infectious)	0.11685	0.1
η	Natural mortality rate (unrelated to epidemic)	5	2.4559
ϑ	Relapse rate (recovered-to-susceptible)	0.01	0.1
ν	Progression rate (exposed-to-infectious)	0.4	0.1
ζ	Recovery rate	0.3	1
$\mathfrak{d}$	Disease-specific mortality rate	0.5	0.1
γ	Fractional order (indicates memory effect)	0.98	0.995
$\mathtt{S}(0)$	Initial condition (susceptible population)	2	3
$\mathtt{E}(0)$	Initial condition (exposed population)	1	4
$\mathtt{I}(0)$	Initial condition (infectious population)	1	3
$\mathtt{R}(0)$	Initial condition (recovered population)	1	2

1. Disease-Free Equilibrium (DFE) Case

   In this scenario, we analyze the finite-time stability around the Disease-Free Equilibrium (DFE) point, defined by $\mathcal{E}_0$. We set the parameters in the table above, ensuring they meet the stability criteria for demonstrating finite-time stability at the DFE.

   (a) Setup and Equilibrium Definition

   For the SEIR model with fractional order γ, the DFE can be defined as $\mathcal{E}_0 = (\mathtt{S}^*, \mathtt{E}^*, \mathtt{I}^*, \mathtt{R}^*)$, where:

$$\mathtt{S}^* = \frac{\lambda}{\eta} = 0.02, \quad \mathtt{E}^* = 0, \quad \mathtt{I}^* = 0, \quad \mathtt{R}^* = 0. \tag{50}$$

   This state indicates no current infection in the population and is essential for proving the model's stability under epidemic control measures.

   (b) Finite-Time Stability Analysis

   We define a Lyapunov function $\mathtt{V}(\mathrm{t})$ based on the deviations of S, E, I, and R from their equilibrium values as in equation (40):

$$\mathtt{V}(\mathrm{t}) = \frac{1}{2}\left(|\mathtt{S}(\mathrm{t}) - 0.02|^2 + \mathtt{E}^2(\mathrm{t}) + \mathtt{I}^2(\mathrm{t}) + \mathtt{R}^2(\mathrm{t})\right). \tag{51}$$

   We then calculate the fractional derivative ${}_0^C D_{\mathrm{t}}^{\gamma}\mathtt{V}(\mathrm{t})$ and demonstrate that this derivative is negative around $\mathcal{E}_0$, confirming stability. If conditions like (36)-(39) hold:

$$\mathtt{N}(\mathrm{t}) \geq 1, \tag{52}$$

$$\Lambda^* = \min\left\{\eta - \frac{\vartheta}{2} - \frac{(\mathsf{C}_1 + \mathsf{C}_2)\max\{\mathfrak{r}_1, \mathfrak{r}_2\}}{4\mathtt{N}^*}, \eta + \frac{\nu}{2} - \frac{(2\mathsf{C}_1 + \mathsf{C}_2)\max\{\mathfrak{r}_1, \mathfrak{r}_2\}}{8\mathtt{N}^*}, \right.$$
$$\left. \mathfrak{d} + \eta + \frac{\zeta - \nu}{2} - \frac{\mathsf{C}_2\max\{\mathfrak{r}_1, \mathfrak{r}_2\}}{8\mathtt{N}^*}, \eta + \frac{\vartheta - \zeta}{2}\right\} = 2.0445375 > 0. \tag{53}$$

   where $\mathsf{C}_1 = \max\{\ell_1^*, \mathtt{S}^*\} = 1.0100$ and $\mathsf{C}_2 = \max\{\ell_2^*, \mathtt{S}^*\} = 1.0100$, given that

$$\mathtt{E}(\mathrm{t}) < \ell_1^* = 1.0100, \quad \mathtt{I}(\mathrm{t}) < \ell_2^* = 1.0100. \tag{54}$$

   Furthermore, the estimated settling time is given by

$$\mathfrak{t}_{\mathfrak{e}1} = \left(\frac{\gamma + 1}{\Lambda^*}\right)^{\frac{1}{\gamma - 1}} = 4.971580969498518s. \tag{55}$$

   we conclude finite-time stability by showing that $\mathtt{V}(\mathrm{t})$ converges to zero as

$$\mathrm{t} \to \mathfrak{t}_{\mathfrak{e}1} = 4.971580969498518s.$$

(c) Validation with Simulation

We simulate the fractional-order system numerically using initial conditions close to the DFE, observing how quickly $\mathtt{E}(\mathtt{t})$, $\mathtt{I}(\mathtt{t})$, and $\mathtt{R}(\mathtt{t})$ approach zero. This supports the model's finite-time stability and alignment with Theorem 4.3.

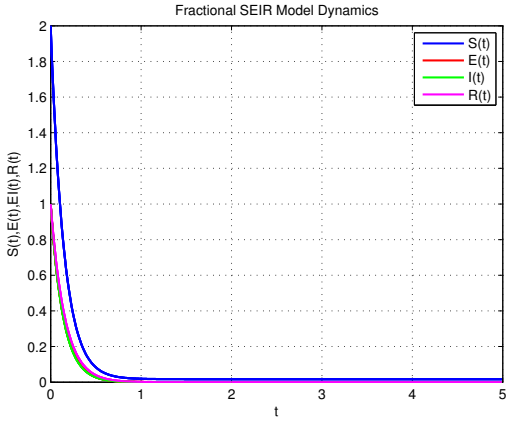

Figure 1: Numerical simulation of $\mathtt{S}(\mathtt{t}), \mathtt{E}(\mathtt{t}), \mathtt{I}(\mathtt{t}), \mathtt{R}(\mathtt{t})$ over time $\mathtt{t} \in [0, 5]$.

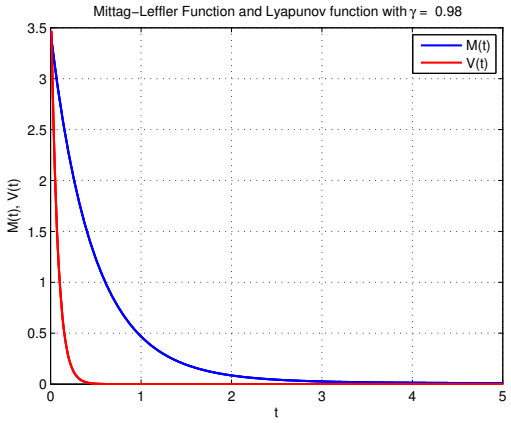

Figure 2: Estimation of the Mittag-Leffler function and Lyapunov function.

2. Pandemic Fixed Point (PFP) Case

This example explores finite-time stability around the Pandemic Fixed Point, where infections are present but controlled.

(a) Setup and Equilibrium Definition

We define the Pandemic Fixed Point (PFP) $\mathcal{E}_1^* = (\mathtt{S}_1^*, \mathtt{E}_1^*, \mathtt{I}_1^*, \mathtt{R}_1^*)$ as:

$$\mathtt{E}^* = 8.8657 \times 10^{-5},\ \mathtt{I}_1^* = \frac{\nu}{\zeta + d + \eta}\mathtt{E}^* = 2.2104 \times 10^{-10},\ \mathtt{R}_1^* = \frac{\zeta \mathtt{I}_1^*}{\eta + \vartheta} = 7.3558 \times 10^{-11},$$
$$\mathtt{S}_1^* = \frac{\lambda + (\zeta\vartheta - (\eta + \nu))\mathtt{E}^*}{\eta} = 1.2215, \tag{56}$$

where $\mathcal{E}_1^*$ represents the exposed population at equilibrium, and $\mathtt{S}_1^*$, $\mathtt{E}_1^*$, $\mathtt{I}_1^*$, and $\mathtt{R}_1^*$ satisfy the SEIR model's constraints.

(b) Finite-Time Stability Analysis

We construct a Lyapunov function for deviations from the PFP, ensuring that $\mathtt{V}(\mathtt{t})$ is positive definite. We then calculate ${}_0^C D_{\mathtt{t}}^{\gamma} \mathtt{V}(\mathtt{t})$ and demonstrate that it satisfies the stability condition, decreasing over time under conditions specified in Theorem 4.3:

$$\mathtt{N}(\mathtt{t}) \geq 2, \tag{57}$$

$$\Lambda^* = \min\left\{\eta - \frac{\vartheta}{2} - \frac{(\mathsf{C}_1+\mathsf{C}_2)\max\{\mathfrak{r}_1,\mathfrak{r}_2\}}{4\mathtt{N}^*}, \eta + \frac{\nu}{2} - \frac{(2\mathsf{C}_1+\mathsf{C}_2)\max\{\mathfrak{r}_1,\mathfrak{r}_2\}}{8\mathtt{N}^*},\right.$$
$$\left.\mathfrak{d} + \eta + \frac{\zeta-\nu}{2} - \frac{\mathsf{C}_2\max\{\mathfrak{r}_1,\mathfrak{r}_2\}}{8\mathtt{N}^*}, \eta + \frac{\vartheta-\zeta}{2}\right\} = 2.0059 > 0. \tag{58}$$

where $\mathsf{C}_1 = 4.0100$ and $\mathsf{C}_2 = 3.0100$, given that

$$\mathtt{E}(\mathtt{t}) < \ell_1^* = 4.0100, \quad \mathtt{I}(\mathtt{t}) < \ell_2^* = 3.0100. \tag{59}$$

Furthermore, the estimated settling time is given by

$$\mathtt{t}_{\mathfrak{e}2} = \left(\frac{\gamma+1}{\Lambda^*}\right)^{\frac{1}{\gamma-1}} = 2.973552902523773s. \tag{60}$$

(c) Validation with Simulation

We simulate the system starting near the PFP, adjusting fractional-order γ and observing system behavior over time. The goal is to confirm that the infection levels $\mathtt{E}(\mathtt{t})$, $\mathtt{I}(\mathtt{t})$, and $\mathtt{R}(\mathtt{t})$ stabilize at non-zero values, consistent with the theoretical predictions.

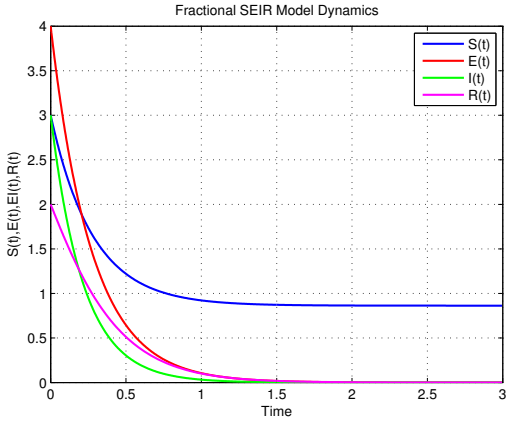

Figure 3: Numerical simulation of $\mathtt{S}(\mathtt{t}), \mathtt{E}(\mathtt{t}), \mathtt{I}(\mathtt{t}), \mathtt{R}(\mathtt{t})$ over time $\mathtt{t} \in [0, 3]$.

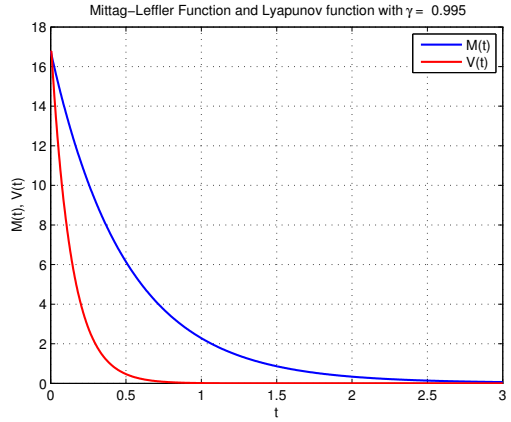

Figure 4: Estimation of the Mittag-Leffler function and Lyapunov function.

6 Conclusion

This study has comprehensively analyzed a fractional-order SEIR model to explore the dynamics of infectious diseases, specifically COVID-19, by integrating memory effects through fractional derivatives. Incorporating fractional-order calculus has enabled a deeper understanding of disease transmission, recovery, and mortality rates while addressing complex dynamics often observed in real-world epidemic scenarios.

Key findings of this research include:

1. **Stability Analysis:** The disease-free equilibrium (DFE) and the pandemic fixed point (PFP) were rigorously analyzed for finite-time stability using Lyapunov functions. Critical conditions for achieving stability were identified, offering insights into disease eradication or control under different parameter configurations.
2. **Numerical Simulations:** The theoretical findings were validated through simulations, demonstrating the finite-time stabilization around equilibrium points. The results showcased the influence of fractional orders on disease progression and underscored the practical utility of fractional-order modeling in capturing real-world epidemic dynamics.
3. **Model Applicability:** The fractional-order SEIR model provided enhanced accuracy compared to traditional integer-order models, particularly in scenarios involving memory effects and anomalous diffusion. This highlights the model's potential for informing public health strategies and intervention planning.

This work emphasizes the value of fractional-order modeling in epidemic dynamics, presenting a robust framework for analyzing disease behavior and evaluating control measures. Future research could extend this approach to explore more complex disease models, incorporate additional real-world parameters, and develop optimized intervention strategies to mitigate epidemic impacts. Additionally, integrating network-based models with fractional-order frameworks could provide further insights into interconnected population dynamics and policy effectiveness.

References

[1] M. Singh, D. Dev, A recent review on: Coronavirus disease 2019, Asian Journal of Pharmacy and Clinical Research, vol. 15, no. 7, 2022.

[2] T. Singhal, A review of coronavirus disease-2019 (COVID-19), Indian Journal of Pediatrics, vol. 87, no. 3, pp. 281-286, 2020.

[3] D. Prathumwan, K. Trachoo, I. Chaiya, Mathematical modeling for prediction dynamics of the coronavirus disease 2019 (COVID-19) pandemic, quarantine control measures, Symmetry, vol. 12, no. 9, article 1404, 2020.

[4] R. Pastor-Satorras, C. Castellano, P. V. Mieghem, A. Vespignani, Epidemic processes in complex networks, Reviews of Modern Physics, vol. 87, no. 3, pp. 925-979, 2014.

[5] A. B. Gumel, E. A. Iboi, C. N. Ngonghala, E. H. Elbasha, A primer on using mathematics to understand COVID-19 dynamics: modeling, analysis, and simulations, Infectious Disease Modelling, vol. 6, no. 1, pp. 148-168, 2020.

[6] M. E. Mehdi, S. Khelifa, O. Bounedjah, M. Rachik, Modeling and analysis of a fractional order spatio-temporal SEIR model: stability and prediction, Results in Control and Optimization, vol. 2024, article 100433.

[7] A. Lamamri, I. Jebril, Z. Dahmani, A. Anber, M. Rakah, S. Alkhazaleh, Fractional calculus in beam deflection: analyzing nonlinear systems with Caputo and conformable derivatives, AIMS Mathematics, vol. 9, no. 8, pp. 21609-21627, 2024.

[8] A. Bataihah, Some fixed point results with application to fractional differential equation via new type of distance spaces, AIMS Mathematics, vol. 7, no. 3, pp. 202-208, 2024.

[9] T. Anderson, J. Yu, A. Züfle, The 1st ACM SIGSPATIAL International Workshop on Modeling and Understanding the Spread of COVID-19, SIGSPATIAL Special, vol. 12, pp. 35-40, 2021.

[10] C. Kresin, F. P. Schoenberg, G. O. Mohler, Comparison of Hawkes and SEIR models for the spread of COVID-19, Advances in Applied Statistics, 2022.

[11] N. Gunasekaran, R. Vadivel, G. Zhai, S. Vinoth, Finite-time stability analysis and control of stochastic SIR epidemic model: a study of COVID-19, Biomedical Signal Processing and Control, vol. 86, pp. 105123, 2023.

[12] H. Singh, H. M. Srivastava, Z. Hammouch, K. S. Nisar, Numerical simulation and stability analysis for the fractional-order dynamics of COVID-19, Results in Physics, vol. 20, pp. 103722, 2020.

[13] Z. Feng, Z. Xiang, Finite-time stability of equilibrium point of a class of fractional-order nonlinear systems, Journal of the Franklin Institute, vol. 361, pp. 106753, 2024.

[14] J. Jiang, H. Li, K. Zhao, et al., Finite-time stability and sliding mode control for uncertain variable fractional order nonlinear systems, Advances in Difference Equations, vol. 2021, pp. 127, 2021.

[15] M. B. Trawicki, Deterministic SEIRS epidemic model for modeling vital dynamics, vaccinations, and temporary immunity, Mathematics, vol. 5, pp. 7, 2017.

[16] Y. Zhang, X. Yu, H. Sun, G. R. Tick, W. Wei, B. Jin, COVID-19 infection and recovery in various countries: modeling the dynamics and evaluating the non-pharmaceutical mitigation scenarios, arXiv: Populations and Evolution, 2020.

[17] A. Grant, Dynamics of COVID-19 epidemics: SEIR models underestimate peak infection rates and overestimate epidemic duration, medRxiv, 2020.

[18] W. S. Hart, M. Bynum, C. D. Laird, J. D. Siirola, A. Staid, Large-scale nonlinear approaches for inference of reporting dynamics and unobserved SARS-CoV-2 infections, Sandia National Laboratories, 2021.

[19] M. E. Mehdi, K. Sofiane, B. Omar, R. Mostafa, Modeling and analysis of a fractional order spatio-temporal SEIR model: stability and prediction, Results in Control and Optimization, 2024.

[20] L. Zhang, M. U. Rahman, Q. Haidong, M. Arfan, Adnan, Fractal-fractional anthroponotic cutaneous leishmania model study in sense of Caputo derivative, Alexandria Engineering Journal, 2021.

[21] Q. Haidong, M. U. Rahman, M. Arfan, G. Laouini, A. Ahmadian, N. Senu, S. Salahshour, Investigating fractal-fractional mathematical model of tuberculosis (TB) under fractal-fractional Caputo operator, Fractals, 2022.

[22] R. Saadeh, M. A. Abdoon, A. M. Qazza, M. Berir, F. E. Guma, N. Al-Kuleab, A. Degoot, Mathematical modeling and stability analysis of the novel fractional model in the Caputo derivative operator: a case study, Heliyon, vol. 10, 2024.

[23] C. Li, Y. Q. Chen, J. Kurths, Fractional calculus and its applications, Philosophical Transactions of the Royal Society A: Mathematical, Physical and Engineering Sciences, vol. 371, 2013.

[24] J. Shen, J. Lam, Non-existence of finite-time stable equilibria in fractional-order nonlinear systems, Automatica, vol. 50, pp. 547–551, 2014.

[25] Z. Feng, Z. Xiang, Finite-time stability of fractional-order nonlinear systems, Chaos, vol. 34, no. 2, 2024.

[26] F. Wang, D. Chen, X. Zhang, Y. Wu, Finite-time stability of a class of nonlinear fractional-order system with the discrete-time delay, International Journal of Systems Science, vol. 48, pp. 984–993, 2017.

[27] Y. Ke, Finite-time stability of fractional order BAM neural networks with time delay, Journal of Discrete Mathematical Sciences and Cryptography, vol. 20, pp. 681–693, 2017.

[28] F. H. Clarke, Yu. S. Ledyaev, Mean value inequalities, Proceedings of the American Mathematical Society, vol. 122, no. 4, pp. 1075–1083, 1994.

[29] G. Farraj, B. Maayah, R. Khalil, W. Beghami, An algorithm for solving fractional differential equations using conformable optimized decomposition method, International Journal of Advances in Soft Computing and Its Applications, vol. 15, no. 1, 2023.

[30] M. Berir, Analysis of the effect of white noise on the Halvorsen system of variable-order fractional derivatives using a novel numerical method, International Journal of Advances in Soft Computing and Its Applications, vol. 16, no. 3, pp. 294–306, 2024.